Progress In Electromagnetics Research, Vol. 122, 389–411, 2012

OPTIMIZED LOCAL SUPERPOSITION IN WIRELESS SENSOR NETWORKS WITH T-AVERAGE-MUTUAL-COHERENCE

D. Guo, X. Qu, L. Huang*, and Y. Yao

Department of Communication Engineering, Xiamen University, Xiamen 361005, China

Abstract—Compressed sensing (CS) is a new technology for recovering sparse data from undersampled measurements. It shows great potential to reduce energy for sensor networks. First, a basic global superposition model is proposed to obtain the measurements of sensor data, where a sampling matrix is modeled as the channel impulse response (CIR) matrix while the sparsifying matrix is expressed as the distributed wavelet transform (DWT). However, both the sampling and sparsifying matrixes depend on the location of sensors, so this model is highly coherent. This violates the assumption of CS and easily produces high data recovery error. In this paper, in order to reduce the coherence, we propose to control the transmit power of some nodes with the help of t-average-mutual-coherence, and recovery quality are greatly improved. Finally, to make the approach more realistic and energy-efficient, the CIR superposition is restricted in local clusters. Two key parameters, the radius of power control region and the radius of local clusters, are optimized based on the coherence and resource consideration in sensor networks. Simulation results demonstrate that the proposed scheme provides a high recovery quality for networked data and verify that t-average-mutual-coherence is a good criterion for optimizing the performance of CS in our scenario.

1. INTRODUCTION

Low cost sensors can be deployed in the environment for object tracking, surveillance, control, etc. Since energy and bandwidth are scarce resources in sensor networks, it is important to design an energy efficient data collection method for wireless sensor networks.

Received 26 July 2011, Accepted 23 November 2011, Scheduled 5 December 2011

* Corresponding author: Lianfen Huang (lfhuang@xmu.edu.cn).

Given the low power of radio at each node, only a small fraction of nodes will find themselves within transmission range of the fusion center. A simple way is that each node transmits its own samples to the fusion center via data hoping. Another method is to group the nodes into clusters and perform data aggregation for the sensors in each cluster [1]. This scheme exploits locally spatial correlation of networked data to reduce the number of bits to be transmitted to the fusion center.

Recently, compressed sensing (CS) [2, 3] provides a very different approach for data sampling and compression in wireless sensor networks [4–8], remote sensing [9, 10] and medical imaging [11]. The main idea of CS is that any unknown signal $\mathbf{x}$ having a sparse representation in one basis (sparsifying transform) can be recovered from a small number of projections onto a second basis (sampling matrix) which is incoherent with the first one.

Successful application of CS requires two key tenets: sparsity and incoherence. In this paper, assuming that the networked data are sparse in a given transform, e.g., distributed wavelet transform (DWT), we propose a power control scheme to reduce the coherence between the sampling matrix (for global superposition) and the sparsifying matrix (for the distributed wavelet transform). We observe that the power control is necessary to significantly reduce the data recovery error. T-average-mutual-coherence is adopted to estimate two key parameters, $d_{\min}$ and $d_{\max}$, in the proposed schemes considering data recovery quality and energy consumption. Besides, we found that restricting the wireless superposition in local clusters will significantly save energy and keep high recovery quality. Simulation results demonstrate that the proposed scheme provides well recovered networked data.

The remainder of the paper is organized as follows. Section 2 introduces the theoretical background of CS and the related applications in sensor network. In Section 3, the proposed system models are proposed. How the proposed system works and how to optimize two important parameters to provide low error recovered data are also discussed. Section 4 gives simulation results. Discussion of the proposed system is given in Section 5. Finally, Section 6 concludes the paper.

2. BACKGROUND OF CS

Under CS framework, the measurements of $\mathbf{x}$ are $\mathbf{y} = \Phi\mathbf{x}$, where $\Phi \in \mathbb{R}^{M\times N}$ is a sampling matrix with far fewer rows than columns ($M \ll N$). The measurement $\mathbf{y} \in \mathbb{R}^M$ is much easier than the original networked data $\mathbf{x} \in \mathbb{R}^N$ to be stored, transmitted, and retrieved since

$M \ll N$.

Let $\Psi \in \mathbb{R}^{N\times N}$ be a transform matrix, the representation of $\mathbf{x}$ in Ψ domain is,

$$\mathbf{x} = \Psi\alpha. \tag{1}$$

If $\|\alpha\|_0 \ll N$, we call α the sparse representation of $\mathbf{x}$. Therefore, the measurements can be expressed as,

$$\mathbf{y} = \Phi\Psi\alpha. \tag{2}$$

The vector α can be accurately recovered from $\mathbf{y}$ as the unique solution to

$$\hat{\alpha} = \arg\min_\alpha \|\alpha\|_1 \quad \text{s.t.} \quad \mathbf{y} = \Phi\Psi\alpha \tag{3}$$

if $\mathbf{A} = \Phi\Psi$ satisfies the restricted isometry property (RIP) [3] condition.

Definition of RIP [3]: For each integer $s = 1, 2, \ldots$, define the isometry constant δ_s of a matrix $\mathbf{A}$ as the smallest number such that

$$(1-\delta_s)\|\alpha\|_2^2 < \|\mathbf{A}\alpha\|_2^2 < (1+\delta_s)\|\alpha\|_2^2 \tag{4}$$

holds for all s-sparse vectors α that satisfies $\|\alpha\|_0 = s$. When this property holds (δ_s is not too close to 1), $\mathbf{A}$ approximately preserves the Euclidean length of s-sparse signals α, so that one can hope to reconstruct α.

The RIP property of $\mathbf{A}$ can guarantee the exact recovery of original signal $\mathbf{x}$ from measurements $\mathbf{y}$. In reality, it is difficult to verify RIP in polynomial time due to its combinatorial flavor [12]. Alternatively, mutual coherence provides a measure of the worst similarity between the columns, as such two closely related columns may confuse any pursuit technique [13]. However, mutual coherence does not do justice to the actual behavior of sparse representations and the performance of pursuit algorithms. Instead, Elad [13] proposed an "average" measure of coherence, which is more likely to describe the true behavior of sparse representations and the performance of pursuit algorithms.

Definition of t-averaged mutual-coherence (TAMC) [13]: TAMC is defined as the average of all absolute normalized inner products between different columns in $\mathbf{A}$ (denoted as $\nu_{i,j}$) that are above threshold t. Put formally,

$$\mu_t\{\mathbf{A}\} = \frac{\sum_{1\le i,j\le N, i\ne j}(\nu_{i,j} \ge t)\cdot\nu_{i,j}}{\sum_{1\le i,j\le N, i\ne j}(\nu_{i,j} \ge t)} \tag{5}$$

where the value of threshold t is known and fixed, $\mu_{0.2}\{\mathbf{A}\} > t$. Typically $t = 0.2$ [13], and we denote the average mutual-coherence of those above 0.2 by $\mu_{0.2}\{\mathbf{A}\}$.

In sensor network, sampling matrix $\mathbf{\Phi}$ is usually pre-designed, e.g., each sensor locally draws M elements of the random projection

vectors by using its network address as the seed of a pseudorandom number generator. Based on the CS theory, Jia et al. [8] consider a sparse event detection scenario where the channel impulse response (CIR) matrix is used as a natural sampling matrix. Another attractive technique delivers random projections of the networked data by exploiting uncoded (analog) coherent transmission [4, 6, 8, 14], which requires only one transmission per random projection. From the nodes in the network to the receiver, the CS projections are simultaneously calculated (by the superposition of radio waves) and communicated directly in the air interface using amplitude-modulated coherent transmissions of randomly weighted sensed values.

The original networked data $\mathbf{x}$ may be sparse itself or can be sparsified with a suitable transform. One example of the self-sparse $\mathbf{x}$ in sensor network is the sparse event detection where most of the entries in $\mathbf{x}$ are non-zeros [8]. Usually, the networked data vector $\mathbf{x}$ is sparse with a proper Ψ in Equation (1). Most of the previous works [7, 15, 16] consider a regular sensor network. However, sensors are usually deployed on an irregular grid. So it is expected to find some sparse representations to sparsify irregular grid sensor networked data.

3. PROPOSED METHODS

In this paper, we consider a scenario where sensor nodes are deployed in an irregular grid. Aiming at improving the data recovery quality,= and reducing the network energy consumption, three system models are proposed to generate random projections of networked data by exploiting uncoded coherent transmission within CS framework. The three models are as follows:

1) Basic CIR model. It uses CIR matrix as the sampling matrix and Distributed Wavelet Transform (DWT) matrix as the sparsifying transform matrix. However, the large mutual coherence between CIR matrix and DWT matrix results in large recovery error of the networked data. Basic CIR model is a highly coherent model.
2) Low-coherent CIR (LC-CIR) model. It reduces the coherence of the basic model by controlling the transmission power of some nearest nodes around projection nodes, which significantly reduces the recovery error.
3) Low-coherent Local CIR (LCL-CIR) model. CIR is restricted in local clusters to save channel estimation and communication cost, and the recovery error is still acceptable. The wedding of power control and local CIR makes this model more efficient.

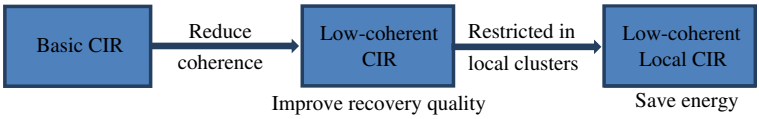

Figure 1. Logic flow of designing the three models.

The logic flow of designing the three models is summarized in Figure 1. In the following, we will analyze each model, make comparisons in terms of recovered data quality, and optimize two key parameters $d_{\min}$ and $d_{\max}$ using TAMC.

3.1. Basic CIR Model

Consider the basic CIR model as shown in Figure 2. There are N sensors randomly located in a field, each generating a data sample to be measured x_j $(j = 1, \ldots, N)$. These data samples $\mathbf{x} = [x_1, \ldots, x_N]$ are called networked data [4], which will be transmitted to the fusion center. $M = O(s \log N)$ sensors are chosen from N sensors as projection nodes. They capture the random linear projections from N sensors.

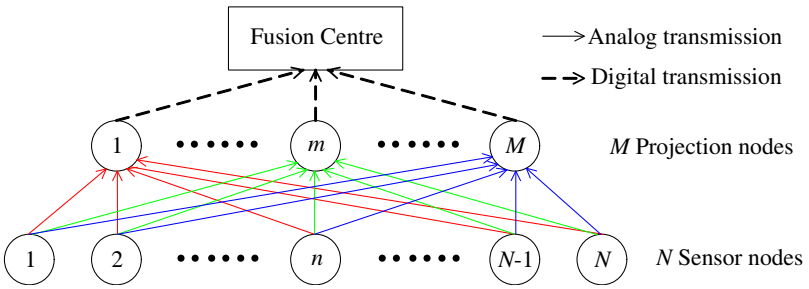

Figure 2. The basic CIR model.

Before proceeding further, we shall make the following assumptions:

1) The locations of the sensors are fixed and known a priori.
2) Networked data vector is sparse or highly compressible in DWT domain, i.e., it contains s largest coefficients. Setting the rest coefficients zero will not cause much information loss.
3) The CIR of each link between projection node and any sensor is known at the fusion center.

4) Each sensor has a local oscillator synchronized to the carrier frequency f_c, and the network is distributed phase synchronized in the sense that the sensor transmissions arrive at the projection nodes in a phase coherent fashion.

3.1.1. Basic CIR

In the basic CIR model, all sensors simultaneously broadcast a piece of data with the same transmission power P_t. As a result, at every projection node, the received signals are simultaneously added in air by the superposition of radio waves, i.e., analog modulated signals are interfering with each other, and also deteriorated by propagation loss and thermal noise. The received signal vector can be written as,

$$\mathbf{y} = \mathbf{G}\mathbf{x} \tag{6}$$

where $\mathbf{G}$ is the CIR matrix whose component can be written as

$$\mathbf{G}(m,n) = (d_{m,n})^{-\beta} |h_{m,n}| \tag{7}$$

where $d_{m,n}$ is the distance between the mth projection node and the nth sensor node. β is the propagation loss factor which is 2 for free space [8, 17] and other values for different scenarios [17, 18]. $h_{m,n}$ is the Raleigh fading modeled as complex Gaussian noise with zero mean and unit variance [8]. The coherent receptions for each projection node are none-interfering, which may be achieved via time-division. Thus, $\mathbf{G}$ depends on the network topology.

Matrix $\mathbf{G}$ exploits the average property of multiple access control and nature of broadcasting in wireless channel. The channel estimation methods can be found in [19, 20] and the references in them. Phase coherent reception can be accomplished either through training-based channel estimation for stationary channels or at a small cost of SNR degradation by employing differential encoding for a fast fading channel [21].

3.1.2. DWT Basis

Distributed wavelet transform (DWT) [22] is successfully applied to sparsify the network data [4, 22] acquired by the sensors deployed in an irregular grid. Once the fusion center knows the locations of all sensor nodes, DWT basis can be computed. The DWT basis will not change if the sensors locations do not change. The DWT basis only depends on network topology. Given a time snapshot of a measured spatial field, DWT replaces the 2-D set of measurements with a set of transform coefficients that, for piecewise smooth fields, are sparser than the original data,

$$\mathbf{x} = \mathbf{D}\boldsymbol{\alpha} \tag{8}$$

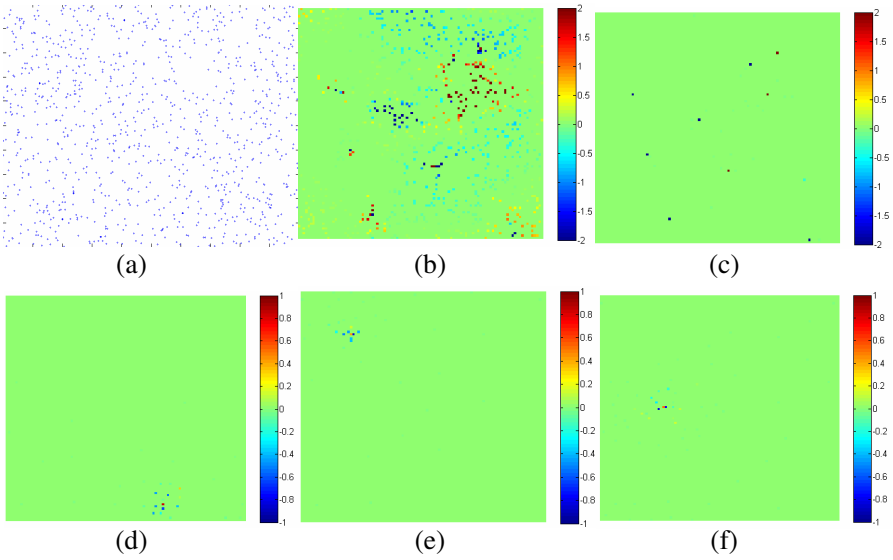

Figure 3. Sparsity of networked data in a DWT basis. (a) Network topology comprised of 1000 nodes, (b) networked data, (c) coefficients after DWT transform, (d)–(f) are three atoms of DWT basis which are localized. Note: The field size in Figure 2(a) is $R \times R = 100 \times 100\,\mathrm{m}$ with $N = 1000$ sensors. The number of nonzero wavelet coefficients in Figure 2(c) is $s = 10$. Note: The locations of nodes are generated as random values drawn from the standard uniform distribution on the open interval (0, 100).

where $\mathbf{x} \in \mathbb{R}^N$ represents the original networked data, $\boldsymbol{\alpha} \in \mathbb{R}^N$ the transform coefficient vector which contains $s\,(s \ll N)$ nonzeros, and $\mathbf{D} \in \mathbb{R}^{N \times N}$ the DWT basis.

For example, a sensor network contains 1000 nodes in Figure 3(a), whose networked data shown in Figure 3(b), can be sparsely represented by the DWT coefficients in Figure 3(c). Three columns (atoms) of $\mathbf{D}$ shown in Figures 3(d)–(f) imply that DWT basis is localized. This localization property comes from the principle of DWT for networked data [22].

3.1.3. Data Recovery

Incorporating the DWT basis, the basic CIR model can be expressed as,

$$\mathbf{y} = \mathbf{GD}\boldsymbol{\alpha} \tag{9}$$

In this model, CIR matrix is employed as a natural CS sampling matrix to obtain the M random projections of the networked data. The measurements $\mathbf{y}$ are sequentially received at the projection nodes. Then, all projection nodes transmit measurements to the fusion center independently. Finally, the fusion center decodes the N dimensional vector $\mathbf{x} = \mathbf{D}\alpha$ from the M dimensional vector $\mathbf{y}$.

Within the CS framework, the sparse coefficients α are estimated by solving the ℓ_1 norm minimization problem

$$\hat{\boldsymbol{\alpha}} = \arg\min_{\boldsymbol{\alpha}} \|\boldsymbol{\alpha}\|_1 \quad \text{s.t.} \quad \mathbf{y} = \mathbf{GD}\boldsymbol{\alpha} \tag{10}$$

so that one can recover the network data $\hat{\mathbf{x}} = \mathbf{D}\hat{\boldsymbol{\alpha}}$.

Successful recovery of $\hat{\boldsymbol{\alpha}}$ relies on the RIP condition in Equation (6). As stated in Section 2, the TAMC of $\mathbf{A} = \mathbf{GD}$ can be used to analyze the behavior of sparse representations data recovery.

Recovery error of networked data from $M = 200$ measurements

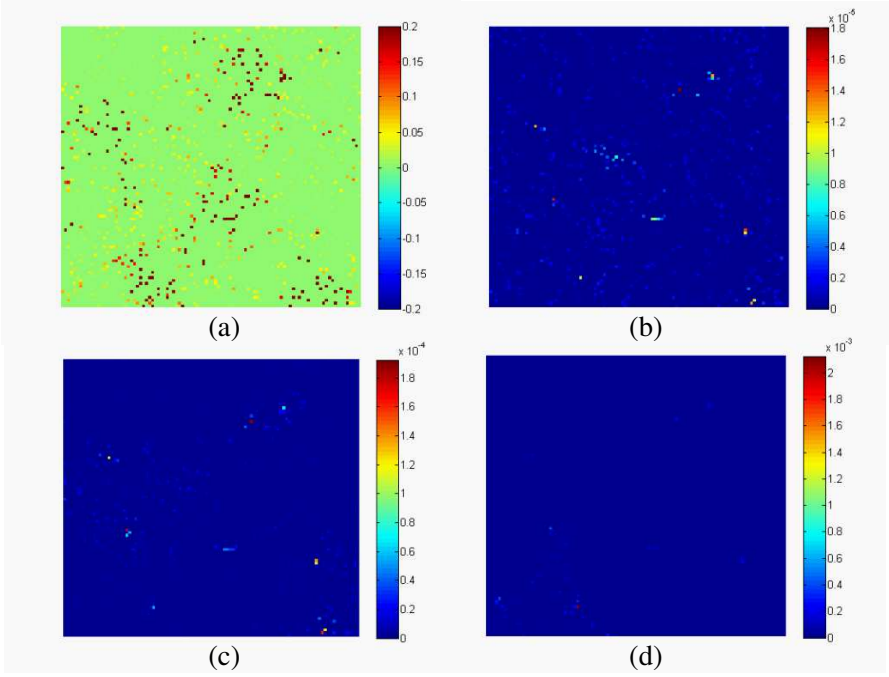

Figure 4. The recovery errors of different models. (a) Error of the basic CIR model ($d_{\min} = 0$ and $d_{\max} = 50$). (b) Error of the LC-CIR model with lowest coherence ($d_{\min} = 50$ and $d_{\max} = 50$). (c) Error of the LC-CIR model ($d_{\min} = 10$ and $d_{\max} = 50$). (d) Error of the LCL-CIR model ($d_{\min} = 10$ and $d_{\max} = 15$).

is really large as shown in Figure 4(a) for a given deployed sensors in Figure 3(a), although $s = 10$ nonzero wavelet coefficients can sparsely represent the network data. The computed TAMC is $\mu_{0.2}\{\mathbf{A}\} = \mu_{0.2}\{\mathbf{GD}\} = 0.51$, which is large.

Intuitively, both $\mathbf{G}$ and $\mathbf{D}$ matrixes depend on network topology and present localization property: neighboring nodes have large weights while distant nodes have small weights. This is why the basic CIR model is highly-coherent.

3.2. Low-coherent CIR Model

In this subsection, we will discuss how to design a proper $\mathbf{A}$ to achieve low coherence thus reduce the recovery error.

Ideally, if the term $(d_{m,n})^{-\beta}$ in Equation (6) is removed (saying $\beta = 0$), the $|h_{m,n}|$ will generate a random matrix composed of complex Gaussian noise with zero mean and unit variance. Random matrix has low coherence with any other sparsifying matrix [2–4]. The coherence $\mu_{0.2}(\mathbf{A})$ is reduced to 0.26 shown in Table 1. Accordingly, very low recovery error is achieved in Figure 4(b) for $\beta = 0$. This example points out the way to reduce the coherence of $\mathbf{A}$, that is breaking the localization property caused by β in matrix $\mathbf{G}$.

Table 1. T-averaged mutual-coherence (TAMC) for the proposed models.

Model	Sensing matrix $\mathbf{A}$	$\mu_{0.2}(\mathbf{A})$	Recovered error
Basic CIR	$\mathbf{G} \times \mathbf{D}$	0.51	Figure 4(a)
LC-CIR (lowest coherence)	$\mathbf{G} \times \mathbf{P} \times \mathbf{D}$	0.26	Figure 4(b)
LC-CIR	$\mathbf{G} \times \mathbf{P}_L \times \mathbf{D}$	0.30	Figure 4(c)
LCL-CIR	$\mathbf{G}_L \times \mathbf{P}_L \times \mathbf{D}$	0.32	Figure 4(d)

Since the nodes are static, the location of sensors will not change, and both $\mathbf{G}$ and $\mathbf{D}$ will not change either. In order to reduce the coherence, we design a control matrix,

$$\mathbf{P}_{m,n} = (d_{m,n})^{\beta} \tag{11}$$

to reduce the TAMC of $\mathbf{A}$. By multiplying $\mathbf{P}_{m,n}$ and $\mathbf{G}_{m,n}$, we have $\mathbf{P}_{m,n} \times \mathbf{G}_{m,n} = |h_{m,n}|$ which can successfully eliminate the localization property of $\mathbf{G}$. The realization of $\mathbf{P}$ in sensor network is to control the transmission power from sensor nodes to projection nodes.

To reduce the number of nodes which require power control, we restrict the power control in a circle with radius $d_{\min}$, centered at a

projection node. The received signal vector can be written as,

$$\mathbf{y} = \mathbf{G}\mathbf{P}_L\mathbf{x} = \mathbf{G}\mathbf{P}_L\mathbf{D}\boldsymbol{\alpha} = \mathbf{A}\boldsymbol{\alpha} \tag{12}$$

where $\mathbf{P}_L$ represents the local power control matrix, whose components can be represented as,

$$\mathbf{P}_L(m,n) = \begin{cases} \left(\frac{d_{m,n}}{d_{\min}}\right)^{\beta}, & d_{m,n} < d_{\min} \\ 1, & \text{otherwise} \end{cases}. \tag{13}$$

When $d_{m,n} < d_{\min}$, the transmit power is set as $(\frac{d_{m,n}}{d_{\min}})^{\beta}$. When $d_{m,n} \geq d_{\min}$, $\mathbf{P}_L(m,n) = 1$ means no power control. After reducing the transmission power, the nodes whose distance is smaller than $d_{\min}$ are conceptually located at the circle of $d_{\min}$, as illustrated in Figure 5.

The power control matrix $\mathbf{P}_L$ can compensate the localization property of sensing matrix $\mathbf{G}$. This leads to reduced coherence of system $\mathbf{A} = \mathbf{G}\mathbf{P}_L\mathbf{D}$ as shown in Table 1. Thus the data recovery error has been greatly reduced, as shown in Figure 4(c) for $d_{\min} = 10\,\text{m}$. Conceptually, we can view that these controlled sensors are located at the circle of $d_{\min}$ although they are physically located inside the circle.

3.3. Low-coherent Local CIR Model

The global superposition scheme uses $\mathbf{G}$ as sampling matrix, and the channel estimation cost scales up with the number of sensors [19]. Ensuring coherent reception of the whole network is also challenging in practice due to tight synchronization requirements.

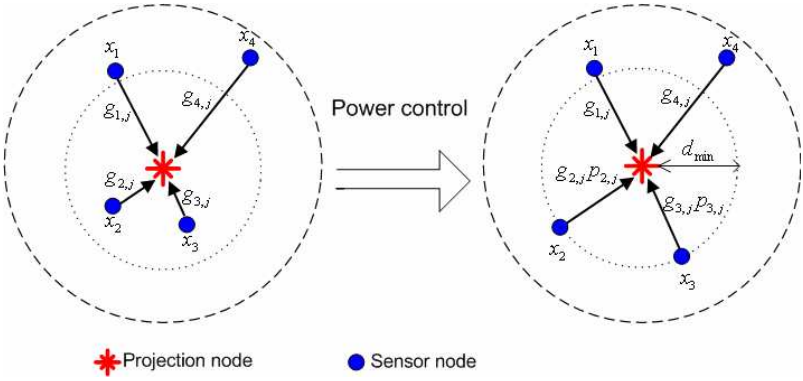

Figure 5. Transmission power control. The nodes inside the radius $d_{\min}$ needs power control. After power control, the equivalent distances of these nodes become $d_{\min}$.

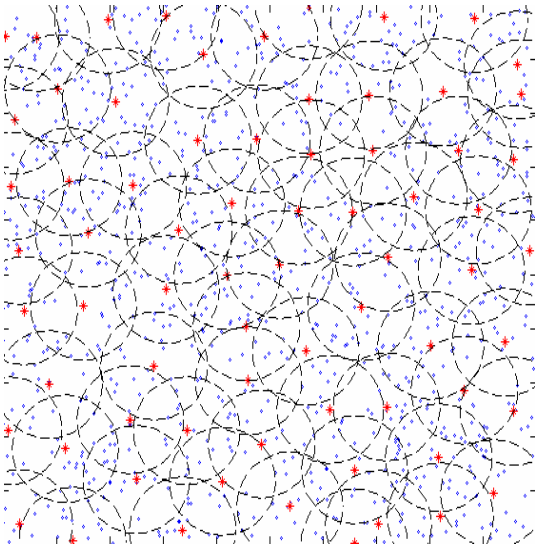

Figure 6. Low-coherent Local CIR (LCL-CIR) model. Each circle represents one cluster where "·" denotes the sensor node and "∗" denotes the projection node which is responsible to transmit the measurements of its cluster to fusion center. Note: The locations of nodes are generated as random values drawn from the standard uniform distribution on the open interval (0, 100).

To release these burdens, we propose local superposition for the sensors within local clusters. Both phase coherent reception and channel estimation are limited in local clusters, making it much easier to realize. We define the sensors in the cluster as $\Omega(m)$. Any nodes $\forall n \in \Omega(m)$ simultaneously transmit their samples to mth projection node. The radius of $\Omega(m)$ is $d_{\max}$. Other nodes outside $\Omega(m)$ do not transmit their samples to mth projection node. Suppose that $\mathbf{G}_L$ is the local CIR matrix, whose component can be written as,

$$\mathbf{G}_L(m,n) = \begin{cases} |h_{m,n}| \left(d_{m,n}\right)^{-\beta}, & d_{m,n} \le d_{\max} \\ 0, & \text{otherwise} \end{cases} \tag{14}$$

The neighboring clusters are overlapped with each other as shown in Figure 6.

In the LCL-CIR model, each projection node obtains one measurement, i.e., a weighted sum of sample values from local sensors. This is illustrated in Figure 7. In order to avoid interference between clusters, local superposition happens sequentially among clusters. The

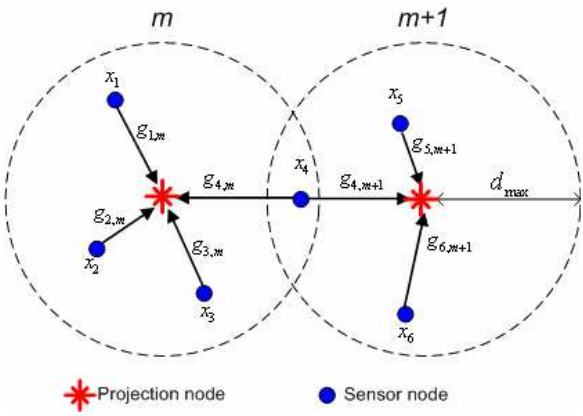

Figure 7. Local superposition in clusters. The radius of $\Omega(m)$ is $d_{\max}$. Sensor nodes $\forall n \in \Omega(m)$ transmit their samples to mth projection node. Then, Sensor nodes $\forall n \in \Omega(m+1)$ transmit their samples to $(m+1)$th projection node.

received signal vector can be written as,

$$\mathbf{y} = \mathbf{G}_L \mathbf{P}_L \mathbf{x} = \mathbf{G}_L \mathbf{P}_L \mathbf{D} \boldsymbol{\alpha} \tag{15}$$

Multiplying $\mathbf{G}_L$ and $\mathbf{P}_L$ we have

$$(\mathbf{G}_L \mathbf{P}_L)_{m,n} = \begin{cases} |h_{m,n}| \, (d_{\min})^{-\beta}, & d_{m,n} \leq d_{\min} \\ |h_{m,n}| \, (d_{m,n})^{-\beta}, & d_{\min} \leq d_{m,n} \leq d_{\max} \\ 0, & \text{otherwise} \end{cases} \tag{16}$$

Figure 4(d) demonstrates that the recovery error of LCL-CIR model is also very low since the coherence is low.

To sum up, we design to control the transmission power of some nearest nodes to reduce the mutual coherence of the sensing matrix. Also, local CIR can reduce the channel estimation cost and keep the recovery error under a low level. The whole process is summarized in algorithm I.

3.4. Optimization of $d_{\min}$ and $d_{\max}$

3.4.1. Energy Model

For the LCL-CIR model, there are two key parameters: $d_{\min}$ and $d_{\max}$. How can we optimize the values for $d_{\min}$ and $d_{\max}$ to balance the recovery quality, channel estimation cost, and power control cost? In this paper, TAMC is adopted as a criterion to optimize $d_{\min}$ and $d_{\max}$ aiming at low coherence which can result in low recovery error.

Algorithm I. Optimized local superposition in sensor networks

Initialization:

1) N sensors transmit their locations to fusion center;
2) Fusion center computes DWT basis $\mathbf{D}$;
3) Set $d_{\max}$: optimize $d_{\max}$ by balancing TAMC and the channel estimation cost which satisfies $E_{ce} \propto d_{max}^4$;
4) Set $d_{\min}$: optimize $d_{\min}$ by balancing TAMC and the power control cost which satisfies $E_{pc} \propto d_{min}^2$;
5) Fusion center chooses M projection nodes from N sensors.

Main:

For $m = 1, \ldots, M$,
6) mth projection node sequentially broadcast its location.
7) Other nodes compute the distance $d_{m,n}$.
8) Power control according to Equation (13).
9) Local superposition according to Equation (14).
10) mth projection node sent its measurement to fusion center.
End
11) Fusion center decodes α from measurements $\mathbf{y}$ according to Equation (10).

Output: $\hat{x} = \mathbf{D}\hat{\alpha}$.

Assume that N nodes are distributed uniformly in a $R \times R$ region with M projection nodes as the cluster-head. The node density is ρ_0. The total energy of the local CIR model can be estimated by,

$$E_{\text{total}} = E_{pc} + E_{tr} + E_{ce} \tag{17}$$

where E_{pc}, E_{tr} and E_{ce} are the energy consumptions on power control, transmission and channel estimation for all nodes.

In order to estimate E_{pc}, let the power control area be a circle with radius $d_{\min}$ and centered at a projection node. The number of nodes which need power control in one cluster is $\rho_0 \pi d_{\min}^2$. Assuming that power control of each node is equal, E_{pc} is

$$E_{pc} = M \times c_1 \rho_0 \pi d_{\min}^2 \tag{18}$$

where M is the number of clusters, and c is a constant. As a result, the energy consumption for power control satisfies $E_{pc} \propto d_{\min}^2$.

In order to estimate E_{tr}, let $d_{\max}$ be the radius of each cluster, and the number of sensors in one cluster is $\rho_0 \pi d_{\max}^2$. According to the first order radio model described in [1], E_{tr} is proportional to the square sum of the distances between all node pairs,

$$E_{tr} = M \times c_2 \sum\nolimits_{i=1}^{I} d_{i,j}^2 = M \times c_2 \times \rho_0 \pi d_{\max}^2 \times E\left\{d_{toCH}^2\right\}. \tag{19}$$

where $E\{d_{toCH}^2\}$ is the expected squared distance from the nodes to the cluster-head (assume to be at the center of the mass of the cluster) [1].

For the node distribution $\rho(x, y)$ in an arbitrary area, $E\{d_{toCH}^2\}$ is

$$E\left\{d_{toCH}^2\right\} = \iint \left(x^2 + y^2\right) \rho(x, y) dx dy = \iint r^2 \rho(r, \theta) r dr d\theta. \quad (20)$$

If we assume that this area is a circle with radius $R = d_{\max}$ and that $\rho(r, \theta)$ is constant for r and θ, this equation is simplified to

$$E\left\{d_{toCH}^2\right\} = \rho \int_{\theta=0}^{2\pi} d\theta \int_{r=0}^{d_{\max}} r^3 dr = \frac{\pi \rho d_{\max}^4}{2} \quad (21)$$

If the density of the nodes is uniform throughout the cluster area, then

$$\rho = \frac{1}{\pi d_{\max}^2} \quad (22)$$

and

$$E\left\{d_{toCH}^2\right\} = \frac{d_{\max}^2}{2}. \quad (23)$$

Therefore, the transmission energy for all nodes is

$$E_{tr} = M \times c_2 \rho_0 \frac{\pi d_{\max}^4}{2}. \quad (24)$$

As a result, the energy consumption for transmission satisfies $E_{tr} \propto d_{\max}^4$.

The energy consumption for channel estimation is denoted as E_{ce}. Every node needs to transmit a pilot signal to the cluster-head, and the cluster-head measures the received signal of each link [19]. According to the radio energy model in Equation (19), E_{ce} is also proportional to the square sum of the distances between all node pairs,

$$E_{ce} = M \times c_3 \sum\nolimits_{i=1}^{I} d_{i,j}^2 = M \times c_3 \rho_0 \frac{\pi d_{\max}^4}{2} \quad (25)$$

The energy consumption for channel estimation satisfies $E_{ce} \propto d_{\max}^4$.

Thus, the total energy is

$$\begin{aligned} E_{\text{total}} &= M \times c_1 \rho_0 \pi d_{\min}^2 + M \times c_2 \rho_0 \frac{\pi d_{\max}^4}{2} + M \times c_3 \rho_0 \frac{\pi d_{\max}^4}{2} \\ &= M \left[c_1 \rho_0 \pi d_{\min}^2 + (c_2 + c_3) \rho_0 \pi d_{\max}^2 E\left\{d_{toCH}^2\right\}\right] \\ &= M \rho_0 \pi \left(c_1 d_{\min}^2 + \frac{c_2 + c_3}{2} d_{\max}^4\right), \end{aligned} \quad (26)$$

where parameters c_1, c_2 and c_3 denote the weights on the energy consumptions in each cluster on channel estimation, power control and transmission, respectively. The values of these parameters depend on realistic scenarios.

3.4.2. Optimization Process

For simplicity, we first optimize $d_{\max}$ and then optimize $d_{\min}$ in two steps:

1) Suppose $d_{\min} = d_{\max}$. This is the ideal case for the sampling matrix, so it is a good start point to optimize $d_{\max}$ by balancing TAMC and the channel estimation cost which satisfies $E_{ce} \propto d_{\max}^4$.
2) Given a fixed $d_{\max}$, $d_{\min}$ is optimized by balancing TAMC and the power control cost which satisfies $E_{pc} \propto d_{\min}^2$.

As shown in Figure 8, when $d_{\max}$ grows, channel estimation cost increases, and TAMC decreases. The crossing point of two curves is

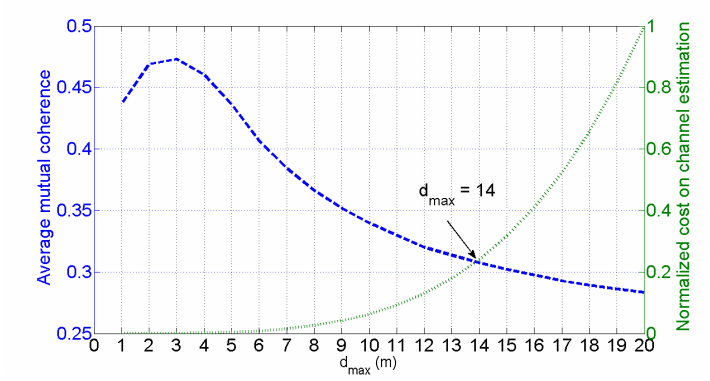

Figure 8. Average mutual coherence ($t = 0.2$) and normalized channel estimation cost in one local superposition for different $d_{\max}$.

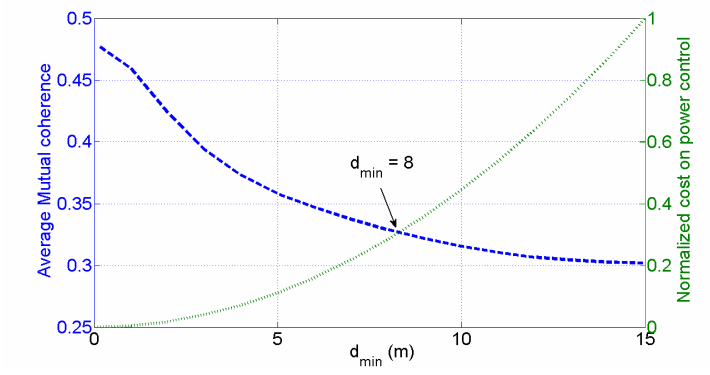

Figure 9. Average mutual coherence ($t = 0.2$) and normalized power control cost in one local superposition whose radius $d_{\max} = 15\,\text{m}$.

at $d_{\max} = 14\,\text{m}$. Since the TAMC cannot fully guarantee the RIP condition, in order to assure the recovery quality, $d_{\max} \geq 14\,\text{m}$ is preferable.

To illustrate the behavior of $d_{\min}$, we provide a demonstration of its results in Figure 9. We set $d_{\max} = 15\,\text{m}$ and use values of $d_{\min}$ from 0 to 15 m. TAMC is decreasing when $d_{\min}$ is growing, and it converges when $d_{\min}$ approaches to $d_{\max}$. The crossing point of two curves is at $d_{\min} = 8\,\text{m}$. This provides a reference value of $d_{\min}$. Since the TAMC cannot fully guarantee the RIP condition, $d_{\min} \geq 8\,\text{m}$ is preferred to improve the recovery quality. The effect of power control and impact of $d_{\min}$ will be demonstrated in the simulation.

4. SIMULATION RESULTS

In this part, we will verify how the proposed scheme can achieve a certain recovery quality after optimizing $d_{\max}$ and $d_{\min}$. In the following simulations, the parameter settings are summarized in Table 2.

Table 2. Parameters setting.

Parameters	**R**	**N**	**s**	**M**	β
Value	100 m	1000	10	200	2

To solve the ℓ_1 norm minimization in Equation (3), the basis pursuit solver in Sparselab toolbox [23] was used. To evaluate recovery quality, we use signal-to-noise ratio (SNR), which is defined as

$$\text{SNR} = 10 \log_{10} \frac{\|\mathbf{x}\|_2^2}{\|\mathbf{x} - \hat{\mathbf{x}}\|_2^2} \tag{27}$$

where $\hat{\mathbf{x}}$ is the recovered data and $\mathbf{x}$ the original data. Higher SNR means lower recovery error.

Based on the observation that 40 dB produces very low recovery error of network data, we set 40 dB as an acceptable threshold of SNR. Figure 10(b) shows the recovered data of original data in Figure 10(a) when SNR is 40 dB. No obvious error is presented in the recovered data as shown in Figure 10(c). When SNR is 30 dB, the error is obvious as shown in Figure 10(e). In the following, the acceptable recovery quality means that the SNR is larger than 40 dB.

4.1. Necessity of Power Control

The necessity of power control is verified in this subsection. Figure 4 shows recovered errors using different models. For the basic CIR model,

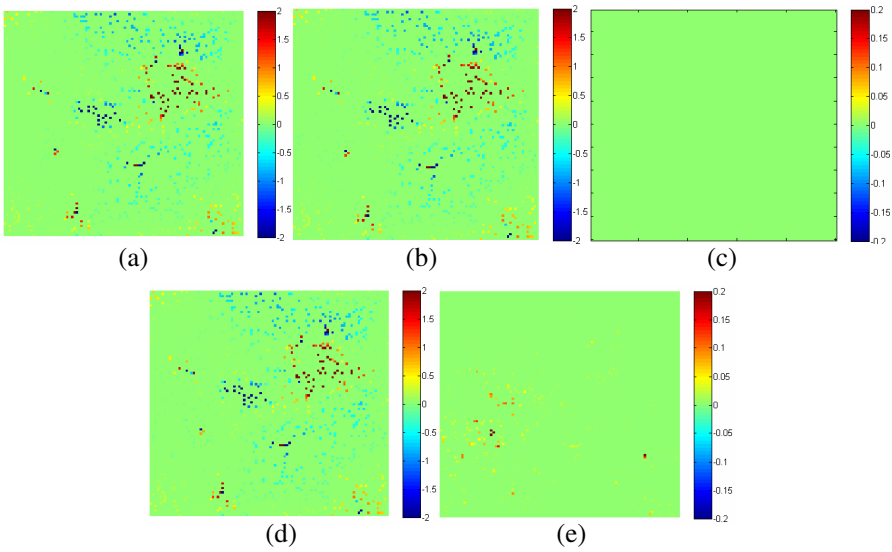

Figure 10. The recovery quality when SNR is 40 dB. (a) Original data. (b) Recovered data with SNR 40 dB. (c) Difference between (a) and (b). (d) Recovered data with SNR 30 dB. (e) Difference between (a) and (d).

no power control is performed, and the errors are large, at the level of 10^{-1}. On the contrary, for the three low-coherent models, the errors are significantly reduced. When power control is performed throughout the whole network, the recovery errors are very small, at the order of 10^{-5}; when power control is restricted to a circle with $d_{\min} = 10$ m, the error is at the order of 10^{-4}. Further, when $d_{\max} = 15$ m, the error is at the order of 10^{-3}.

The results in Figure 4 demonstrate that the construction of matrix $\mathbf{P}$ is necessary to guarantee good quality of recovered data. This necessity does not depend on whether CIR superposition is local or global.

4.2. Effect of $d_{\min}$

The average SNR of the LCL-CIR scheme becomes higher when $d_{\min}$ grows, as shown in Figure 11. To obtain the acceptable SNR, the minimal $d_{\min}$ is 9 m, which is very close to the reference value $d_{\min} = 8$ m in Figure 9. This implies that TAMC is a reasonable criterion to evaluate the true behavior of sparse representations and the performance of the pursuit algorithm in Equation (10).

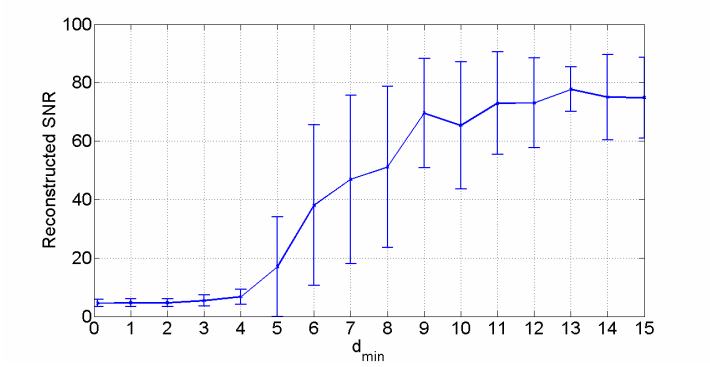

Figure 11. Recovered SNR with different value of $d_{\min}$. Note: The error bar shows the variation of SNR with the random locations of M projection nodes, and $d_{\max} = 15\,\text{m}$.

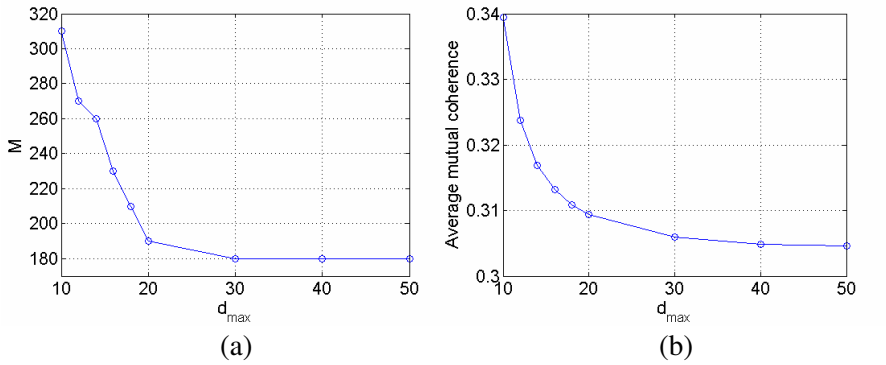

Figure 12. M and TMAC under different value of $d_{\max}$. (a) Required M to achieve acceptable SNR. (b) TMAC when $M = 210$, $d_{\min} = 10\,\text{m}$. Note: (a) is obtained by increasing M so that the lowest SNR is larger than the acceptable SNR 40 dB in 50 repeated simulations.

4.3. Local CIR Versus Global CIR

As stated before, reducing coherence is necessary to reduce the recovery error. Therefore, the discussion of local or global CIR is conducted within LC-CIR model. The global CIR model is a special case of LC-CIR model when $d_{\max}$ is the maximum distance of two nodes in the field.

From the energy analysis in Subsection 3.4.1, the channel estimation cost will be greatly reduced when $d_{\max}$ becomes smaller.

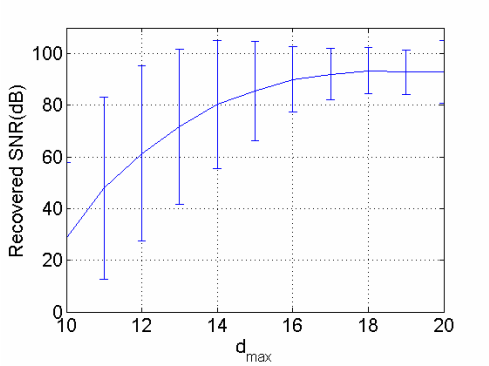

Figure 13. Recovered SNR with different value of $d_{\max}$ when $M = 210$, $d_{\min} = 10\,\text{m}$. Note: The error bar shows the variation of SNR with the random locations of M projection nodes.

However, decrease of $d_{\max}$ requires more clusters, i.e., a larger M to guarantee acceptable recovery quality. As shown in Figure 12(a), for a fixed $d_{\min} = 10\,\text{m}$, when $d_{\max} = 10$, it requires $M = 310$ to obtain acceptable recovery quality, and when $d_{\max} = 20$, $M = 190$ can achieve acceptable recovery quality. The number of measurements approaches to $M = 180$ when $d_{\max} \geq 30$.

When M is fixed, the increase of $d_{\max}$ will decrease mutual coherence between sensing matrix and sparsifying matrix, as shown in Figure 12(b), and thus improve the recovery quality as shown in Figure 13. This observation implies that TAMC is a reasonable criterion to predict data recovery error. For a given realistic scenario, the parameters c_1, c_2 and c_3 may be tested and plugged into Equation (26), then one may optimize $d_{\max}$ to minimize E_{total} and provide small coherence as well.

4.4. Impact of Positioning Error

The impact of positioning error on the low-coherent local CIR model is analyzed from two aspects: 1) how large the position error is and 2) how many nodes positions are corrupted.

The first aspect is simulated by corrupting the ground truth position with random Gaussian noise $\mathcal{N}(0, \sigma^2)$. We choose different σ shown in Table 3 for the $100\,\text{m} \times 100\,\text{m}$ grid where the average distance between two neighboring nodes is 3.4 m.

The second aspect is simulated by randomly choosing partial nodes to be corrupted in positioning. We make 1%, 5%, 10%, 15% and 25% of the node positions corrupted with Gaussian noise.

Table 3. SNR (dB) performance with positioning error.

Position error σ	Ratio of corrupted nodes				
	1%	5%	10%	15%	25%
1×10^{-3}	**80.32**	**74.17**	**64.48**	**71.17**	**64.25**
1×10^{-2}	**60.19**	**49.06**	**41.44**	**42.23**	36.46
1×10^{-1}	**43.35**	30.36	26.71	24.33	21.03
1×10^{0}	27.89	15.97	13.25	11.21	8.63

Positioning errors will reduce the recovery quality using the proposed method. As we discussed before, an acceptable recovery should be with SNR larger than 40 dB. From Table 3, if the position error is relatively small ($\sigma \leq 1 \times 10^{-3}$), nearly 25% nodes are allowed to be with positioning error; if the position error is large ($\sigma \leq 1 \times 10^{-1}$), only 1% of the nodes are allowed to be with positioning error. As a result, right positioning measure is important for the proposed method. Some advanced positioning methods [24–26] may enhance positioning accuracy and thus reduce the reconstruction error.

When the average distance between two neighboring nodes is 3.4 m, the proposed method can overcome large positioning error, if the ratio of corrupted nodes is small (1% of all the nodes).

5. CONCLUSION

We proposed a compressive sensing (CS) scheme based on uncoded coherent transmission in local clusters. CS projection measurements are obtained via the interface of projection nodes and their neighbors. Distributed wavelet transform is used to sparsify irregularly distributed sensor networked data. By controlling transmission power of some nearest neighbors in clusters, the coherence of sampling matrix and sparsifying matrix is reduced. This power control is necessary to significantly reduce the data recovery error. The performance of the data recovery can be enhanced by optimizing the radius of power control region considering the tradeoffs between the t-average-mutual coherence and the energy consumption. Restricting the radius of cluster can save the energy and achieve acceptable data recovery quality. Our method implies that t-average-mutual coherence is a good criterion to show the average behavior of recovery quality.

Limitation of the proposed schemes is that it is sensitive to large positioning error. It is worthwhile to discuss how the variation of density of sensors is in realistic sensor network since in our simulation

the sensors are uniformly distributed in the network. Although the proposed scheme may not be used in real sensor networks right now, the finding of low coherence of sampling and sparsifying matrixes leads to designing more realistic CS schemes in sensor network. In addition, the way reducing the coherence in this paper points out a useful way to reduce the recovery error for a CS system where both sampling matrix and sparsifying matrix are localized.

ACKNOWLEDGMENT

This work was partially supported by Qualcomm-Tsinghua-Xiamen University Joint Research Program and National Natural Science Foundation of China under grant 61172097. Di Guo and Xiaobo Qu would like to acknowledge the fellowship of Postgraduates' Oversea Study Program for Building High-Level Universities from the China Scholarship Council. The authors also thank the reviewers for their thorough review and highly appreciate the comments and suggestions, which significantly contributed to improving the quality of this paper.

REFERENCES

1. Heinzelman, W. B., A. P. Chandrakasan, and H. Balakrishnan, "An application-specific protocol architecture for wireless microsensor networks," *IEEE Trans. Wireless Commun.*, Vol. 1, No. 4, 660–670, 2002.
2. Donoho, D. L., "Compressed sensing," *IEEE Trans. Inf. Theory*, Vol. 52, No. 4, 1289–1306, 2006.
3. Candes, E. J. and M. B. Wakin, "An introduction to compressive sampling," *IEEE Signal Process. Mag.*, Vol. 25, No. 2, 21–30, 2008.
4. Haupt, J., W. U. Bajwa, M. Rabbat, and R. Nowak, "Compressed sensing for networked data," *IEEE Signal Process. Mag.*, Vol. 25, No. 2, 92–101, 2008.
5. Duarte, M. F., S. Sarvotham, D. Baron, M. B. Wakin, and R. G. Baraniuk, "Distributed compressed sensing of jointly sparse signals," *39th Asilomar Conf. Signals, Systems and Computers*, 1537–1541, 2005.
6. Bajwa, W., J. Haupt, A. Sayeed, and R. Nowak, "Compressive wireless sensing," *5th Int. Conf. Information Processing in Sensor Networks*, 134–142, 2006.
7. Lee, S., S. Pattem, M. Sathiamoorthy, B. Krishnamachari, and A. Ortega, "Spatially-localized compressed sensing and routing

in multi-hop sensor networks," *3rd Int. Conf. on Geo. Sensor Networks*, 11–20, 2009.

8. Jia, M., L. Husheng, and H. Zhu, "Sparse event detection in wireless sensor networks using compressive sensing," *43rd Annu. Conf. Information Sciences and Systems*, 181–185, 2009.
9. Wei, S.-J., X.-L. Zhang, J. Shi, and G. Xiang, "Sparse reconstruction for SAR imaging based on compressed sensing," *Progress In Electromagnetics Research*, Vol. 109, 63–81, 2010.
10. Wei, S.-J., X.-L. Zhang, and J. Shi, "Linear array SAR imaging via compressed sensing," *Progress In Electromagnetics Research*, Vol. 117, 299–319, 2011.
11. Zhang, Y., L. Wu, B. Peterson, and Z. Dong, "A two-level iterative reconstruction method for compressed sensing MRI," *Journal of Electromagnetic Waves and Applications*, Vol. 25, No. 8–9, 1081–1091, 2011.
12. Elad, M., *Sparse and Redundant Representations: From Theory to Applications in Signal and Image Processing*, Springer Verlag, 2010.
13. Elad, M., "Optimized projections for compressed sensing," *IEEE Trans. Signal Process.*, Vol. 55, No. 2, 5695–5702, 2007.
14. Gastpar, M. and M. Vetterli, "Power, spatio-temporal bandwidth, and distortion in large sensor networks," *IEEE J. Sel. Areas Commun.*, Vol. 23, No. 4, 745–754, 2005.
15. Guo, D., X. Qu, L. Huang, and Y. Yao, "Sparsity-based spatial interpolation in wireless sensor networks," *Sensors*, Vol. 11, No. 3, 2385–2407, 2011.
16. Quer, G., R. Masiero, D. Munaretto, M. Rossi, J. Widmer, and M. Zorzi, "On the interplay between routing and signal representation for compressive sensing in wireless sensor networks," *Information Theory and Applications Workshop*, 206–215, 2009.
17. Andersen, J. B., T. S. Rappaport, and S. Yoshida, "Propagation measurements and models for wireless communications channels," *IEEE Commun. Mag.*, Vol. 33, No. 1, 42–49, 1995.
18. Gay-Fernandez, J. A., M. Garcia Sanchez, I. Cuiñas, A. V. Alejos, J. G. Sanchez, and J. L. Miranda-Sierr, "Propagation analysis and deployment of a wireless sensor network in a forest," *Progress In Electromagnetics Research*, Vol. 106, 121–145, 2010.
19. Patwari, N. and S. K. Kasera, "Robust location distinction using temporal link signatures," *13th ACM Int. Conf. on Mobile Computing and Networking*, 111–122, 2007.

20. Alsehaili, M., S. Noghanian, A. R. Sebak, and D. A. Buchanan, "Angle and time of arrival statistics of a three dimensional geometrical scattering channel model for indoor and outdoor propagation environments," *Progress In Electromagnetics Research*, Vol. 109, 191–209, 2010.
21. Chen, B., R. Jiang, T. Kasetkasem, and P. K. Varshney, "Channel aware decision fusion in wireless sensor networks," *IEEE Trans. Signal Process.*, Vol. 52, No. 12, 3454–3458, 2004.
22. Wagner, R. S., R. G. Baraniuk, S. Du, D. B. Johnson, and A. Cohen, "An architecture for distributed wavelet analysis and processing in sensor networks," *5th Int. Conf. Information Processing in Sensor Networks*, 243–250, 2006.
23. Donoho, D., V. Stodden, and Y. Tsaig, Sparselab [Online]. Available: http://sparselab.stanford.edu/.
24. Mitilineos, S. A. and S. C. A. Thomopoulos, "Positioning accuracy enhancement using error modeling via a polynomial approximation approach," *Progress In Electromagnetics Research*, Vol. 102, 49–64, 2010.
25. Reza, A. W., S. M. Pillai, K. Dimyati, and K. G. Tan, "A novel positioning system utilizing zigzag mobility pattern," *Progress In Electromagnetics Research*, Vol. 106, 263–278, 2010.
26. Mitilineos, S. A., D. M. Kyriazanos, O. E. Segou, J. N. Goufas, and S. C. A. Thomopoulos, "Indoor localisation with wireless sensor networks," *Progress In Electromagnetics Research*, Vol. 109, 441–474, 2010.